FIELD TRIAL WITH A GSM/DCS1800 SMART ANTENNA BASE STATION

Alexander Kuchar*†, Manfred Taferner*, Michael Tangemann**, and Cornelis Hoek**

* Institut für Nachrichtentechnik und Hochfrequenztechnik
Technische Universität Wien
Gusshausstrasse 25/389, A - 1040 Wien, Austria
** Alcatel Corporate Research Center Stuttgart
D - 70430 Stuttgart, Germany
e-mail: †Alexander.Kuchar@nt.tuwien.ac.at

Abstract – We present measurement results with a GSM1800 smart antenna base station. The base station is equipped with an adaptive antenna array processor that allows in every GSM frame full beam adaptation in uplink and downlink. The smart antenna processing is based on the estimation of the directions of arrival in uplink. It includes separate DOA trackers for uplink and downlink, angular diversity, and beamforming with broad nulls.
Measurements in a static line–of–sight (LOS) scenario demonstrate the potential to suppress interference by $25dB$. The smart antenna achieves a bit–error ratio (BER) of 1% at a carrier–to–interference ratio of $-14dB$. A field measurement in a microcell setup confirms the tracking capability even in scenarios with strong multipath. In a non–LOS situation we achieve an average signal–to–noise gain of $7.4dB$, while it increases up to $8.3dB$ in a LOS environment. The angular diversity concept results in an additional diversity gain of $5.8dB$ at the 1% BER level in case of NLOS when a dual beam configuration is applied.

I. INTRODUCTION

Smart antenna technology is on the brink of commercial realization. Validating concepts by theoretical analysis or by simulation is not enough. Integrating theoretical smart antenna concepts in working solutions and judging their performance in mobile radio channels is today's challenge [1, 2].
We have developed a real–time smart antenna base station. The system works within the GSM standard and is compatible with frequency hopping. In a first stage the smart antenna is used to suppress co–channel interference, i.e. we apply Spatial Filtering for Interference Reduction (SFIR) [3].
We will present how the array processor is embedded into the GSM smart antenna base station.and will summarize the array processing scheme. The focus of this work lies on uplink measurement results. We report on functional tests that were conducted in a controlled environment. The last section presents first field measurement results.

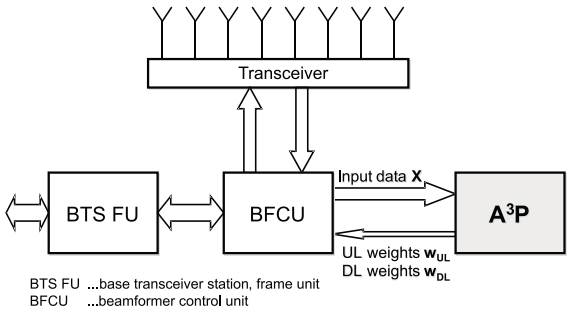

Figure 1: Smart antenna base station.

II. GSM SMART ANTENNA BASE STATION

The test system is based on a standard GSM1800 base station. For smart antenna processing eight transceivers are connected to an antenna array with half wavelength element spacing. All eight downconverted I– and Q–signals are sampled at symbol rate in a beamforming control unit (BFCU). The BFCU collects the samples for each GSM timeslot, and the data of one of the eight timeslots is transferred to the Adaptive Antenna Array Processor **A³P**, which is implemented on a DEC Alpha 500MHz. The processing of the input data matrix $\mathbf{X}$ with a run-time of only $1ms$ allows real-time adaptation of the beamforming weights every GSM frame ($4.6ms$). **A³P**'s processing results in

Figure 2: Measurement setup on the roof top of the Alcatel building. The two mobiles are angularly separated by 19° and have a LOS to the base station array.

weight vectors for the uplink and downlink beamforming. The weight vectors are multiplied with the input data (physical beamforming) in the BFCU. After physical beamforming in the BFCU the user signal is transferred to the baseband detector in the Frame Unit (FU). Similarly the downlink transmitter baseband signal is weighted with the downlink weight vector prior to transmission.

III. THE ADAPTIVE ANTENNA ARRAY PROCESSOR

A³P's processing is based on direction of arrival (DOA) estimation in uplink. The processing is structured in four main sections (for details see [4, 5]):

- DOA estimation: From the received input data in uplink, the number of incoming wavefronts and their DOAs are estimated.
- DOA classification: A user identification algorithm decides whether a wavefront belongs to a user or to an interferer, and the DOAs are correspondingly classified.
- Tracking: The user DOAs are tracked to increase the reliability of the DOA estimates. The tracker precludes far-off estimates from disturbing the beamforming and prevents the DOA estimates from changing too much between two consecutive burst. For uplink and for downlink, separate trackers are used because the averaging in downlink requires larger memory length.
- Signal reconstruction - beamforming: We apply beamforming algorithms in uplink and downlink that place a main beam into the user direction and broad nulls into the directions of interferers [6]. For the uplink we select the user tracker with the strongest *instantaneous* power. Thus *angular diversity* becomes possible, which we implemented. Because the downlink fading is unknown at the base station, the downlink beamformer forms a beam into the direction with the largest *average* power.

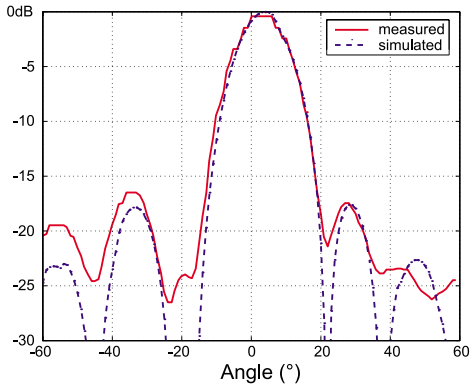

Figure 3: Measured and simulated uplink antenna pattern. The user DOA is $\phi = 0°$, the interferer DOA is $\phi = -19°$.

IV. MEASUREMENTS IN A CONTROLLED ENVIRONMENT

Before performing field measurements, we confirmed the principal functionality of the system in a controlled environment. The array and two mobile stations (MS) antennas were placed on top of the roof of the Alcatel building (Fig. 2). The mobiles had line-of-sight (LOS) to the base station array and were angularly separated by 19°. The measurement scenario was static during the tests.

DOA estimation accuracy and antenna pattern

Functional tests were performed with increasing complexity. First we proved the performance of the various subprocedures of **A³P**, when separated assessment was possible. Starting with the frontend, the DOA estimation, we presented the measured DOA estimation accuracy when a discrete wave is incident from $\phi = 0°$ in [5]. Already with an input signal–to–noise ratio (SNR) of $0dB$ the estimation accuracy is below 1° for all estimators. Next, we measured antenna patterns to assess the capability to suppress interference. The amount of pattern mismatch is a strong indicator for the quality of the calibration. Fig. 3 compares a measured antenna pattern with the theoretical result. Here we applied the beamformer SmearR [6], and assumed that the user DOA is 0° and a single interferer

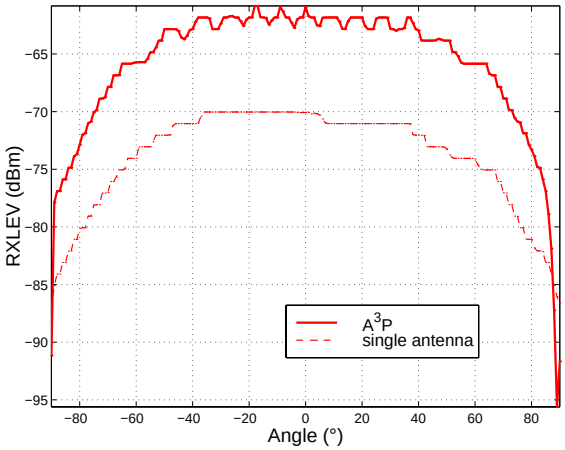

Figure 4: Measured input power over angular range of interest. The antenna array was rotated whereas the MS antenna did not move.

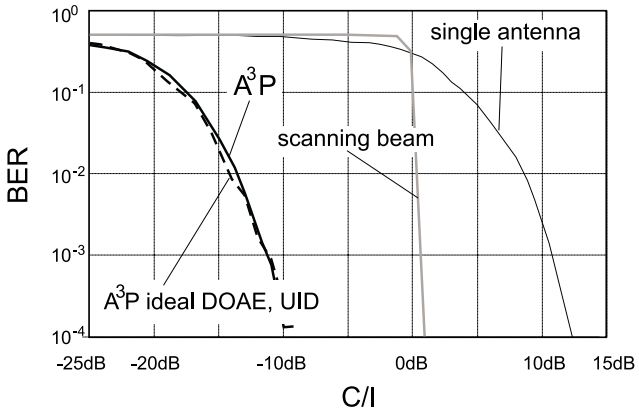

Figure 5: BER of **A³P** in a static channel with continuous wave interferer.

at $\phi = -19°$. The focus in this measurement lay on the broad null that was placed into the interferer direction. The measured pattern showed a null depth, and thus a potential interferer suppression capability, of about $25dB$. This and the excellent agreement between measured and theoretical antenna pattern confirmed the quality of the receivers' calibration.

Finally we checked whether the system was able to track the user DOAs. The antenna array was mounted on a rotor that allows measurements with varying DOAs. We measured the output power of **A³P** for different rotor positions. The resulting gain compared to the single antenna was about $8.5dB$, nearly constant over the entire angular range (Fig. 4).

BER in an AWGN channel with interference

After testing the components of **A³P**'s smart antenna processing, we assessed the whole system. The MS and the base station (BS) were linked via a traffic channel. BER measurements were performed over a period of $10s$ or 2000 bursts. To quantify interference suppression capability, we measured the raw bit-error ratio (BER) of the MS with an interfering continuous wave signal present. The user was positioned at $\phi = 0°$ and had constant power with an input SNR of $28dB$. The interferer, with varying power, was located at $\phi = -19°$. As references we used a scanning beam algorithm and a single antenna. The scanning beam algorithm steers 128 regularly spaced, fixed beams and selects the signal corresponding to the beam that receives most power. Thus it gives satisfying BER only as long as the user signal is stronger than the interferer, i.e. for $C/I > 0dB$. In contrast, **A³P** is much more robust against interference (Fig. 5). It gives a BER of 1% at an input C/I of $-14dB$. Another curve (**A³P** ideal DOAE, UID) quantifies the achievable interference robustness, if the user and interferer DOAs would be known a priori. In this ideal situation, the interference suppression is only limited by the residual imperfections, e.g. receiver phase and amplitude imbalances *after* calibration. In the LOS scenario, **A³P** reaches the optimum performance.

V. FIELD MEASUREMENTS

We now present results from a field measurement in a suburban environment. The array was standing on top of the four storey Alcatel building in Stuttgart, Germany (Fig. 6). The neighboring building is one floor higher than the Alcatel building. Thus a part of the area served by the base station is strongly shadowed. The dashed line in Fig. 6 starting from the array and pointing in about $\phi = 18°$ separates the LOS region (above dashed line) from the NLOS region (below dashed line). The measurement van, equipped with a mobile station, drove in a rectangle along the depicted route. Figure 7 shows the measurement route as seen from the BS array. A part of the route has direct LOS (white arrow). Quasi-LOS situation occured at the last part of the route back to the starting point, where the LOS was obstructed by a building that was lower than the array thus favoring propagation over the roof.

We evaluated the postprocessed output signal after beamforming. Fig. 8 shows the cumulative distribution function (CDF) of the output power of **A³P** compared to the input powers of the eight antenna ele-

Figure 6: Map of measurement route. The array is standing on top of the Alcatel building in Holderäckerstrasse (BS). The van drove a rectangle along the route shown.

ments. We show results for two different **A³P** configurations: in the standard configuration, **A³P** steered a single beam, while in the dual beam configuration **A³P** selected the two user DOAs with largest power. In the latter case beamforming was done for each of the two user DOAs and the output powers were summed up. The average SNR gain of **A³P** in this measurement was $7.4dB$ in the standard configuration. Thus we have included in Fig. 8 a theoretical curve without diversity gain that presents the averaged input antenna power distribution shifted by the average gain. This curve divides the achieved gain into an average SNR gain and into a diversity gain. At the 1% probability level **A³P**'s diversity gain is about $4dB$. The diversity gain is evident from the steeper slope of the CDF of the output power. The scanning beam algorithm that gives the maximum output SNR when considering beam steering, achieves a diversity gain of $2.8dB$ higher than **A³P**. In this measurement the simple scanning beam gives superior performance. But note that **A³P** outperforms this scheme when interference is present (compare Fig. 5). Another curve shows the diversity gain offered by the channel. To get the theoretical optimum output SNR we summed up all input powers, which corresponds to maximum ratio combining. Because **A³P** has the capability to suppress interference, it cannot realize all of the diversity gain offered by the channel.

We summarize the average SNR gains and the SNR gain at the 1% BER level in Tab. 1. Additionally we have divided the measurement route into a LOS and

Figure 7: Measurement route as seen from the array. The van drove along a route that is partially seen from the BS (white line). The inset photo is taken from behind the base station array, looking to the starting point of the measurement route.

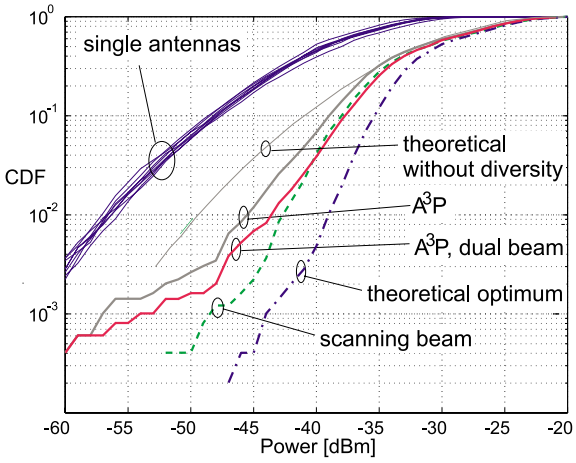

Figure 8: The CDF of the input powers of the eight single antenna elements and the output powers after beamforming (**A³P** and scanning beam). For the theoretical optimum, we summed up the input powers of the single antenna elements.

av. gain [dB]	**A³P**	**A³P**, dual	scan. beam	opt.
LOS	8.1	8.3	8.7	9
NLOS	6.4	7.4	7.1	9
all data	7.4	7.9	8	9
gain at 1%	**A³P**	**A³P**, dual	scan. beam	opt.
LOS	9.3	9.8	11	12.8
NLOS	11.1	13.2	15	20.6
all data	11	12.9	13.8	17.5

Table 1: Average SNR gain and SNR gain at the 1% BER level.

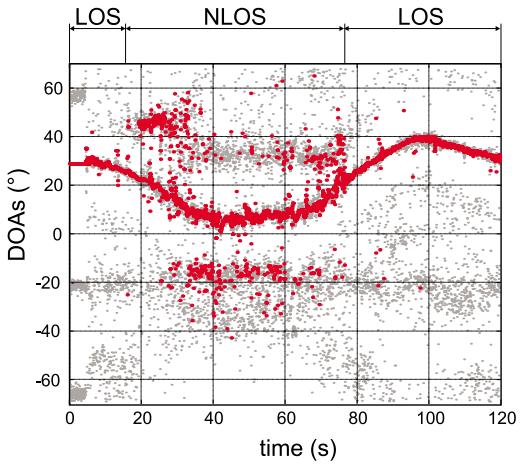

Figure 9: All estimated (gray dots) and the strongest DOAs (black dots) selected in the standard configuration.

an NLOS part, with the NLOS part starting at $15.5s$ and ending at $76.5s$[1].
Finally we plot the DOAs calculated by **A³P** over the period of the measurement (Fig. 9). We compare the estimated DOAs (gray dots) with the user DOAs that were selected for beamforming (larger black dots). The estimated DOAs show, especially during the NLOS period, that significant multipath was present. During this period, the selected user DOA hopped between the multipath components. However, in most cases the LOS direction was selected.
Even in the LOS scenario we found a multipath component at $\phi = -20°$. Because this multipath is evident over the entire measurement route we conclude that it was caused by scattering near the base station — a typical situation in microcell environments.

VI. CONCLUSIONS

The measurements have confirmed the principal functionality of **A³P**. An SNR gain of nearly $8.5dB$ is achievable over the entire angle range in a static scenario. In the same scenario, **A³P** gives a BER of 1% at an input C/I of $-14dB$ thus proving its excellent interference suppression capabilities.

The field measurement with the base station array mounted below roof top of a neighboring building showed:

- **A³P** achieves an average SNR gain of $7.4dB$, even in a NLOS scenario.
- **A³P** is able to track all multipath components, and realizes a diversity gain of $5.8dB$ in a NLOS scenario.
- The tracking scheme is able to follow the movement of the mobile, resulting in a smooth beam steering under LOS situations.

Further measurements with interference will confirm **A³P**'s capability to suppress interference in a mobile radio environment.

Acknowledgment The authors thank Michael Hother and Guillaume de Lattre for operating the measurement equipment, and Prof. Ernst Bonek for encouragement and guidance.

[1] The separation of the LOS from the NLOS measurement is based on the DOA estimates (Fig. 9).

REFERENCES

(1) G. V. Tsoulos, J. P. McGeehan, and M. Beach, "Space division multiple access (SDMA) field trials. part 1: Tracking and BER performance," *IEE Proc. Radar, Sonar and Navigation*, pp. 73–78, Feb. 1998.

(2) B. Hagerman, T. Östman, K. J. Molnar, and G. E. Bottomley, "Field test performance results for D–AMPS in PCS bands with array processing," in *IEEE Vehicular Technology Conference (VTC'97)*, vol. 3, (Phoenix, AZ), pp. 1582–1586, May 1997.

(3) M. Tangemann, C. Hoek, and R. Rheinschmitt, "Introducing adaptive array antenna concepts in mobile communication systems," in *Proc. RACE Mobile Communications Workshop*, (Amsterdam, The Netherlands), pp. 714–727, May 1994.

(4) A. Kuchar, M. Taferner, and E. Bonek, "A run-time optimized adaptive antenna array processor for GSM," in *European Personal Mobile Communications Conference (EPMCC'99)*, (Paris, France), pp. 307–312, Mar. 1999.

(5) A. Kuchar, M. Taferner, M. Tangemann, C. Hoek, W. Rauscher, M. Strasser, G. Pospischil, and E. Bonek, "A robust DOA–based smart antenna processor for GSM base stations," in *IEEE International Conference on Communications (ICC'99)*, (Vancouver, Canada), pp. 11–16, June 1999.

(6) M. Taferner, A. Kuchar, M. Lang, M. Tangemann, and C. Hoek, "A novel DOA–based beamforming algorithm with broad nulls," in *International Symposium on Personal, Indoor and Mobile Radio Communication (PIMRC'99)*, (Osaka, Japan), Sept. 1999.